Flexural Strength of RHS Perforated Lean Duplex Stainless Steel Beam at Temperature 24-900ºC

Priestley, K.A.[1] and Prabowo, A.[1]*

[1] Department of Civil Engineering, Universitas Tarumanagara, INDONESIA

Abstract

The investigation of stainless steel structures at elevated temperatures is still limited, especially to those focused on the behaviour of perforated beams. Therefore, a numerical study was conducted to investigate the behaviour and strength of cold-formed lean duplex stainless steel (CFLDSS) beams having a single web perforation that failed due to pure bending at temperatures between 24-900ºC. In total, 200 square and rectangular hollow sections (RHSs), which had various cross-section sizes, hole diameters, and temperature simulations, were involved in the parametric study. The numerical study was based on the ABAQUS simulation results of the 200 specimens. The numerical model was developed based on the validated existing studies. Numerical evaluations show that the existing codified strength predictions are conservative, but it has inconsistent safety. Hence, this study suggests modifications to the existing strength prediction, which is more conservative and reliable.

Introduction

Apart from wood and concrete, steel is commonly used as structural members in building constructions. Steel construction is relatively faster and more efficient than other construction materials due to its fabrication process. Therefore, steel structures are frequently used in a rapid construction project [1]. Steel profiles can be fabricated and manufactured from two different methods: hot-rolled steel and cold-formed steel. The fabrication and manufacturing processes of hot-rolled steel involve high temperatures, whereas cold-formed steel is manufactured at ambient (normal) temperature.

Today, cold-formed steel does not only apply to carbon steel but also to stainless steel. Because of its corrosion resistance, stainless steel is frequently used. Various grades of stainless steel are available in the market, including lean duplex (EN 1.4162). According to Huang and Young [2], lean duplex stainless steel has a lower price and similar material strength to duplex stainless steel. Therefore, it could attract the construction industry to implement the stainless steel construction on a broader scale [3]. Research and studies on the performance of stainless steel structures have developed in recent years [4].

According to Chen et al. [5], hollow stainless steel beams made of cold-formed steel are frequently used in construction. Additional holes in the web of hollow steel beams, which can be used for electrical routing, pipes and other utilities, will reduce the strength of the beams. When a fire occurs, the strength of perforated stainless steel beams can be further deteriorated. Therefore, the structural design of stainless steel structures must consider fire resistance. The behaviour of RHS (Rectangular Hollow Section) lean duplex stainless steel at extreme temperatures has received little attention, particularly for hollow RHS profiles. As a result, this research aims to propose a computational method applicable to the strength of perforated RHS lean duplex stainless steel beam.

Material Property Modeling

Results from the experimental test conducted by Huang and Young [2] were used to model the material properties of lean duplex stainless steel. Huang and Young [2] propose several parameter coefficient values for this modelling, as shown in Table 1 and Table 2 and Equations (1) – (9).

Table 1. Material Properties of Lean Duplex Stainless Steel at Room Temperature [2]

Type	E (MPa)	f_y (MPa)	f_u (MPa)	ε_u (%)
Lean Duplex	199000	682	828	21.5

Table 2. Coefficient for Lean Duplex Stainless Steel [6, 2]

	T (ºC)	a	b	c	n
E_T	$24 < T \leq 700$	1	24	1384	1
	$700 < T \leq 900$	0.51	700	650	1
$f_{y,T}$	$24 < T \leq 300$	1	24	284	0.75
	$300 < T \leq 600$	0.76	300	2930	1.2
	$600 < T \leq 900$	0.44	600	200	0.75
$f_{u,T}$	$24 < T \leq 400$	0.85	400	3.25×10^8	3
	$400 < T \leq 600$	0.85	400	102560	2
	$600 < T \leq 900$	0.46	600	300	0.83
$\varepsilon_{u,T}$	$22 \leq T < 180$	1	22	480	1
	$180 \leq T < 660$	0.67	180	5.42×10^{21}	8
	$660 \leq T \leq 960$	0.15	660	5000	1

In which, T is the temperature considered as the variation in the study (ºC); a is the coefficient at temperature T; b is the coefficient at temperature T; c is the coefficient at temperature T; n is the coefficient at temperature T.

$$\frac{E_T}{E_0} = a - \frac{(T - b)^n}{c} \tag{1}$$

$$\frac{f_{y,T}}{f_y} = a - \frac{(T - b)^n}{c} \tag{2}$$

$$\frac{f_{u,T}}{f_u} = a - \frac{(T - b)^n}{c} \tag{3}$$

$$\frac{\varepsilon_{u,T}}{\varepsilon_u} = a - \frac{(T - b)^n}{c} \tag{4}$$

In which, E_T is the modulus of elasticity at temperature T (MPa); E_0 is the modulus of elasticity at normal temperature (MPa); $f_{y,T}$ is the yield strength at temperature T (MPa); f_y is yield strength at normal temperature (MPa); $f_{u,T}$ is the ultimate strength at temperature T (MPa); f_u is the ultimate strength at normal temperature (MPa), $\varepsilon_{u,T}$ is the ultimate strain at temperature T (%); ε_u is the ultimate strain at normal temperature (%).

$$\varepsilon_T = \frac{f_T}{E_T} + 0.002 \left(\frac{f_T}{f_{y,T}}\right)^{n_T}, \quad f_T \leq f_{y,T} \tag{5}$$

$$\varepsilon_T = \frac{f_T - f_{y,T}}{E_{y,T}} + \varepsilon_{u,T} \left(\frac{f_T - f_{y,T}}{f_{u,T} - f_{y,T}}\right)^{m_T} + \varepsilon_{y,T}, \quad f_T > f_{y,T} \tag{6}$$

$$E_{y,T} = \frac{E_T}{1 + 0.002 \, n_T \, E_T / f_{y,T}} \tag{7}$$

$$n_T = 6 + 0.2\sqrt{T} \tag{8}$$

$$m_T = 5.6 - \frac{T}{200} \tag{9}$$

In which, ε_T is the strain at temperature T (%); $\varepsilon_{y,T}$ is the strain when the yield strength reaches temperature T (%); f_T is the stress at temperature T (MPa); $E_{y,T}$ is the modulus of elasticity when yield strength reaches temperature T (MPa); n_T and m_T are the coefficient for proposed stress–strain equations above.
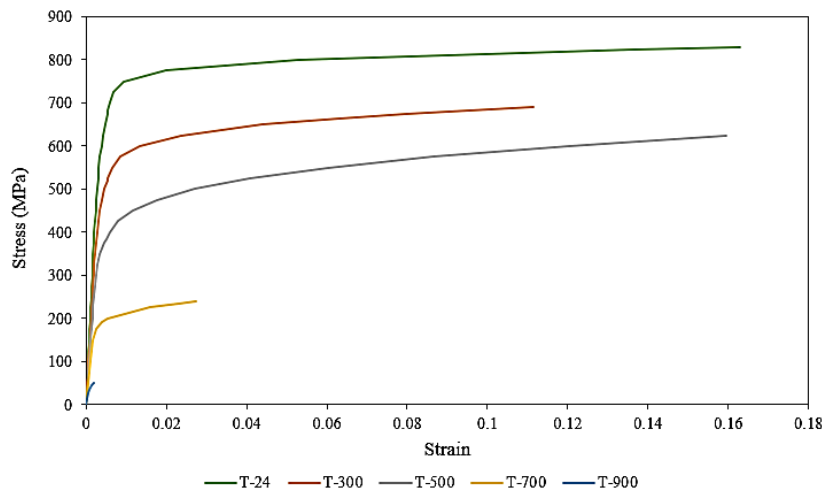
Figure 1. Stress-Strain Curves

After obtaining the stress-strain value (engineering stress-strain) as shown in Figure 1 using Equations (1) – (9), the true stress and logarithmic plastic strain values can be obtained using the Equations (10) and (11):

$$\sigma_{true} = \sigma(1 + \varepsilon) \tag{10}$$

$$\varepsilon^{pl}{}_{true} = ln(1 + \varepsilon) - \frac{\sigma_{true}}{E} \tag{11}$$

In which, σ is the stress (MPa); ε is the strain (%); σ_{true} is the true stress (MPa); $\varepsilon^{pl}{}_{true}$ is the logarithmic plastic strain (%); E is the modulus of elasticity (MPa).

Four-point Bending Test

The four-point bending test produces a constant bending moment in between the two loading points (moment span), while it produces a varying bending moment along the shear span (a distance from the support to the nearest loading point) [7]. The advantages of the four-point bending test are only pure moments and no shear forces occur between the fractured areas [8]. Therefore, an experiment conducted using a four-point bending test setup is suitable for investigating the pure bending strength of cross-sections. The result from the experiment will generate a moment versus curvature curve, where the curvature is calculated using the following equation [9]:

$$k = \frac{1}{r} = \frac{8 (D_M - D_L)}{4(D_M - D_L)^2 + L_2{}^2} \tag{12}$$

In which, k is the curvature (1/mm); r is the radius (mm); D_M is the displacement in the middle of the span (mm); D_L is the average displacement (mm); L_2 is the mid-span length/moment span (mm).

Direct Strength Method

There are two design methods applicable in the current specifications for cold-formed stainless steel design [10]: the effective width method (EWM) and the direct strength method (DSM). The design of cross-sectional strength in EWM is based on the effective properties of sections, which require effective width formulas. When used to calculate the strength of hollow cross-section profiles, this method becomes troublesome [11]. The DSM can be used because it does not require recalculation of cross-sectional properties and effective width formulas, according to Schafer [12]. The DSM, on the other hand, requires a finite strip method program called CUFSM [13] to ease the calculation of elastic buckling capacity. This buckling capacity is critical for calculating the overall cross-sectional strength formula [11].

According to ASCE [10], the flexural strength of doubly-symmetric cross-sections without holes in the web can be determined from the minimum value between the global bending moment (M_{ne}) and the local bending moment (M_{nl}), where:

$$\lambda_l \leq 0.667, M_{nl} = M_{ne} \tag{13}$$

$$\lambda_l > 0.667, M_{nl} = \left[1 - 0.2 \left(\frac{M_{crl}}{M_{ne}}\right)^{0.4}\right] \left(\frac{M_{crl}}{M_{ne}}\right)^{0.4} M_{ne} \tag{14}$$

$$M_{ne} \leq M_y \tag{15}$$

In which, λ_l is the ratio between global bending moment and elastic local bending moment; M_{ne} is the global bending moment (kNm); M_y is the yield moment (kNm); M_{crl} is the elastic local bending moment (kNm); M_{nl} is the nominal moment (kNm). M_{crl} was obtained from the elastic buckling capacity of a cross-section using finite strip analysis. In this study, the CUFSM software built from the study by Schafer and Adany [13], was utilized. For perforated sections, the M_{crl} was determined from the following considerations:

1. If D (hole diameter) $< L_{crlh}$ (half-wave buckling length for perforated sections), the M_{crl} from the signature curve corresponding to L_{crl} (half-wave buckling length for sections wihout a web hole) $= D$ is taken as M_{crlh} (M_{crl} for perforated sections),
2. If $D > L_{crlh}$, the M_{crl} from the signature curve corresponding to $L_{crl} = L_{crlh}$ is taken as M_{crlh},
3. For all possibilities, the value of M_{crlh} shall not be larger than the M_{crl}.

For the RHS section, $M_{ne} = M_y$ because global buckling failure is dominated by local buckling or yielding failure depending on the cross-section slenderness. Torsional buckling does not occur because of the symmetrical shape and high torsional rigidity. Detailed information on how to utilize the CUFSM tool can be found in [14].

Meanwhile, ASCE [10] permits the calculation of the bending strength of the perforated sections using Equations (13) to (15), with the two additional equations below as an additional strength limit.

$$M_{nl} \leq M_{ynet} \tag{16}$$
$$M_{ynet} = S_{fnet}F_y \tag{17}$$

In which, S_{fnet} is the net section modulus (mm³); M_{ynet} is the net section yield moment (kNm). The DSM equation proposed by Chen et al. [5] refers to the AISI specification [15]. The M_{nl} can be determined based on the two equations below:

$$\lambda_l \leq 0.776, M_{nl} = \left(1.5 - \frac{0.5}{0.776}\lambda_l\right)M_{ne} \tag{18}$$

$$\lambda_l > 0.776, M_{nl} = \left[1 - 0.15\left(\frac{M_{crl}}{M_{ne}}\right)^{0.4}\right]\left(\frac{M_{crl}}{M_{ne}}\right)^{0.4}M_{ne} \tag{19}$$

Reliability Analysis

The suitability of the bending strength equation applicable for lean duplex hollow steel beams uses the reliability analysis prescribed in ASCE [10]. The purpose of carrying out the analysis is to obtain a reliability index (β_o) of each design equation being evaluated. A minimum β_o value of 2.5 must be exceeded in order to conclude that the design equation is considered safe. The β_o is obtained from the following equation:

$$\beta_o = \frac{ln\dfrac{C_\phi(M_m F_m P_m)}{\phi}}{\sqrt{V_M{}^2 + V_F{}^2 + C_P V_P{}^2 + V_Q{}^2}} \tag{20}$$

In which, C_ϕ is the calibration coefficient (1.52); M_m is the average value of the material factor (1.10); F_m is the average value of the fabrication factor (1.0); P_m is the average value of the ratio of ultimate capacity to nominal capacity; β_o is the reliability index; V_M is the coefficient of variation of material factors (0.05); V_F is the coefficient of variation of fabrication factors (0.05); C_p is the correction factor $((1 + 1/n)m)/(m - 2)$; n is the number of data; m equals to n - 1; V_p is the coefficient of variation of the ratio of ultimate capacity to nominal capacity, V_Q is the load effect variation coefficient (0.21); ϕ is the strength reduction factor (0.9).

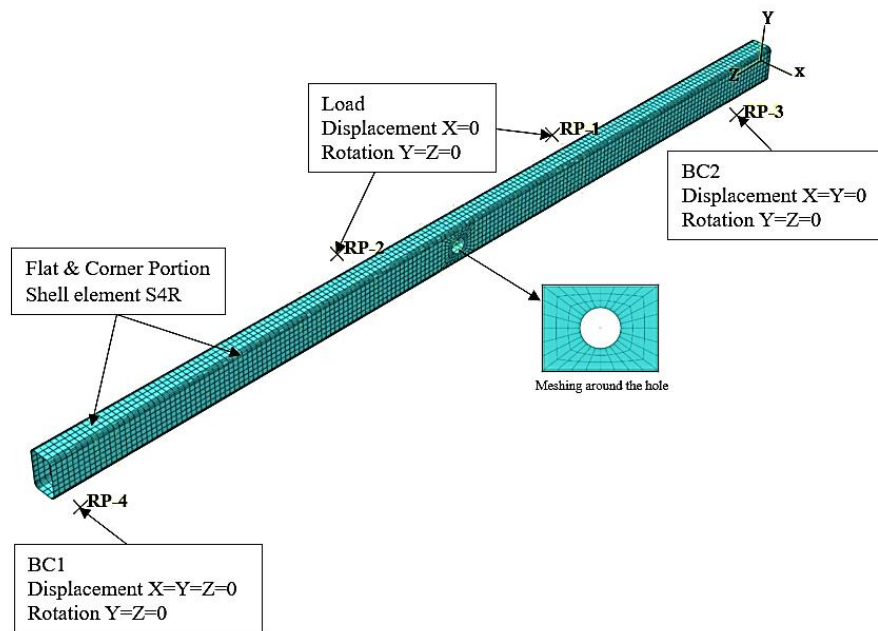## Numerical Modelling and Parametric Study

In this section, the setup of the numerical model of perforated RHS stainless steel beam in ABAQUS [16] is explained. The numerical model closely simulates the four-point bending test conducted by Chen et al. [5]. The model was built using S4R shell elements. The mesh size flat part of the RHS was 7 mm × 7 mm, and the corner part was divided into five elements. The nonlinear material modelling was keyed in from the true stress versus logarithmic plastic strain, as explained in Section 2. The material properties varied depending on the temperature variations being considered. The stress-strain curves for each temperature can be seen in Figure 2.

Mesh refinement was applied to the web hole perimeter. The local and global geometric imperfections were excluded since it was shown by Chen et al. [5] that the imperfections did not have a significant impact on the results of the

simulation. The residual stress was also not incorporated into the model, similar to the FEA of cold-formed lean duplex SS beams at elevated temperatures performed by Huang et al. [17]. Boundary conditions were assigned to the four reference points (RP-1, RP-2, RP-3, RP-4). The reference points were restrained against translation in the X direction and rotation in the Y and Z directions. More detailed information on each boundary condition can be seen in Figure 3. The load was assigned to the numerical model through RP-2 and RP-3 by inserting the target displacement. These four reference points constrained the loading and support area to reflect local cross-sectional restraints in the experiment. The failure of the numerical model mimics the failure of the member under a four-point bending scheme (Figure 4).
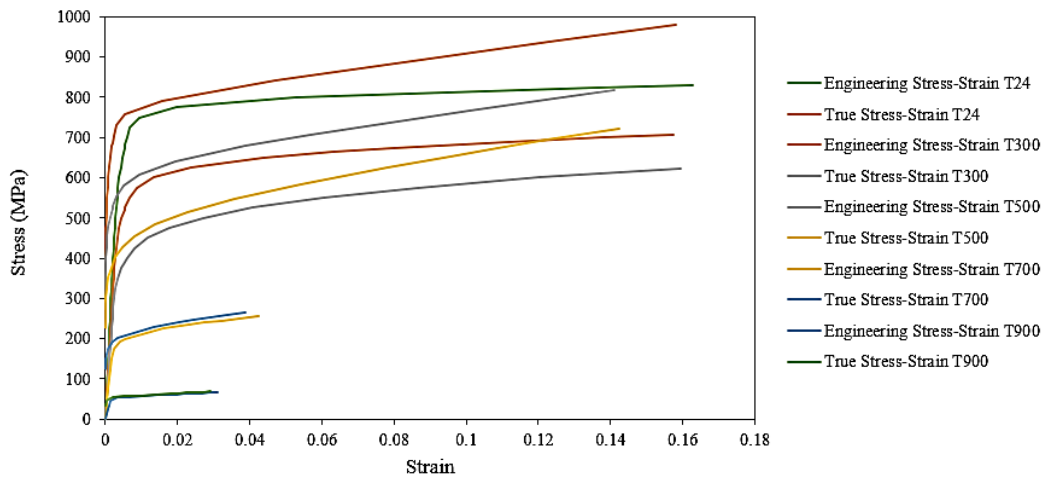
Figure 2. Stress-Strain Curves of Lean Duplex Stainless Steel for Temperature 24ºC–900ºC

Figure 3. Numerical Model of Perforated RHS Beam
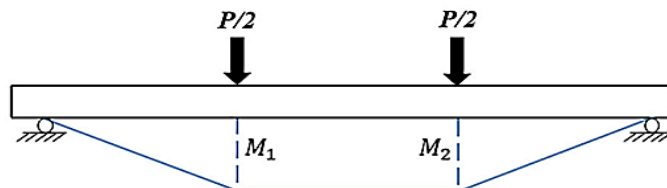
Figure 4. Loading Scheme of Four-point Bending [18]

A parametric study was carried out to obtain the ultimate flexural strength of perforated RHS beams. The study was based on three different variables: cross-section size (see Table 3), hole diameters (see Table 4), and temperature simulation. In total, 200 specimens were built in ABAQUS for the parametric study. The symbols of the cross-section

dimensions are presented in Figure 5. The specimen lengths are further explained in Figure 6. In general, the moment span (L2) is relatively close to the shear span (L1) and ranges between 3H-4H, where H is the overall depth of the cross-section. The hole diameter was calculated based on the percentage values multiplied by the flat depth of the cross-section (h), where h equals $H - 2*(t + r_i)$. The t and r_i are the thickness and internal radius of the cross-section, respectively. Cross-sections without holes were still involved to investigate the strength decrease.
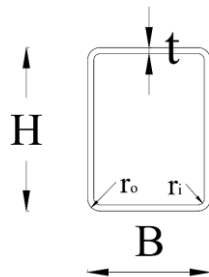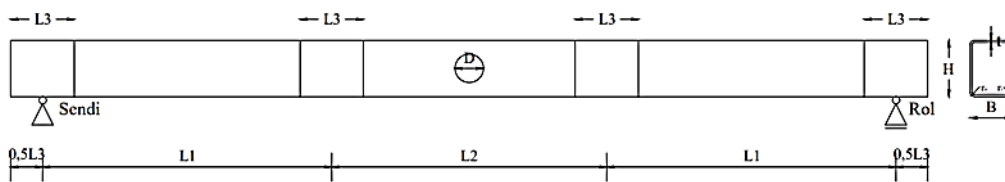

Figure 5. RHS Cross-section

Figure 6. Longitudinal and Transverse Views of the RHS Beam

Table 3. RHS Cross Section Size Details

H (mm)	B (mm)	t (mm)	r_o (mm)	r_i (mm)	L1 (mm)	L2 (mm)	L3 (mm)
60	40	4	7.63	4.44	410	390	90
120	80	3	6.63	4.13	410	390	90
300	120	2	6.5	4.5	1400	1400	350
380	286	2	6.5	4.5	1400	1400	350
380	152	1.5	6.25	4.75	1400	1400	350
380	380	4	7.5	3.5	1400	1400	350
380	570	4	7.5	3.5	1400	1400	350
380	570	2	6.5	4.5	1400	1400	350

Table 4. Hole Size Against Clear Height of RHS Profile Body Plate

No.	Hole Size (D) (%)
1.	0
2.	20
3.	50
4.	70
5.	90

Results and Discussion

Ultimate Flexural Strength (M_{ult})

The pure ultimate bending strength values (M_{ult}) in Table 5 are obtained from ABAQUS results.

The M_{ult} values incorporated the effects of material and geometric nonlinearity considered during analysis in ABAQUS. Thus, the M_{ult} (ultimate moment obtained from ABAQUS) values are equivalent to the nominal capacity of the sections. The overall M_{ult} value is the value of the bending moment on the major axis except for sections 380×570×4 and 380×570×2 due to the value H < B. From Table 5, it can be seen that there is a significant strength reduction at each cross-sectional size where the hole diameter is larger than 20% at all temperatures. However, a negligible strength reduction is seen in the sections with a hole diameter of 20% due to the inherent ductility behaviour of stainless steel.

Table 5. M_{ult} Values of 200 Numerical Specimens

Cross Section (mm)	Hole (%)	M_{ult} (kNm)				
		24ºC	300ºC	500ºC	700ºC	900ºC
60×40×4	D0	10.3	8.8	7.7	3.1	0.8
	D20	10.1	8.5	7.5	3.1	0.8
	D50	9.4	7.8	6.7	2.9	0.8
	D70	8.9	7.4	6.2	2.7	0.7
	D90	8.1	6.7	5.7	2.5	0.7
120×80×3	D0	30.3	23.4	18.0	9.0	2.5
	D20	30.3	23.4	18.0	9.1	2.5
	D50	29.0	23.0	17.7	8.9	2.4
	D70	26.5	21.2	16.1	7.8	2.2
	D90	21.2	14.9	11.3	6.3	1.8
300×120×2	D0	48.7	37.9	28.9	16.3	5.4
	D20	47.3	36.8	28.1	16.0	5.4
	D50	45.4	35.4	27.0	15.4	5.0
	D70	43.0	33.5	25.5	14.4	4.8
	D90	36.2	28.3	21.5	12.3	4.0
380×286×2	D0	73.4	57.0	43.8	25.3	8.1
	D20	68.5	53.4	40.8	23.7	7.5
	D50	67.4	52.3	39.5	23.0	7.2
	D70	65.4	50.3	38.4	21.7	6.5
	D90	54.1	42.2	32.3	18.7	5.7
380×152×1.5	D0	40.1	31.3	23.7	13.4	4.4
	D20	39.4	30.6	23.3	13.3	4.2
	D50	37.5	29.0	22.2	12.7	4.2
	D70	36.0	28.0	21.4	12.0	3.8
	D90	35.7	24.6	18.7	10.3	3.2
380×380×4	D0	290.5	226.1	174.2	110.3	33.8
	D20	289.5	226.1	174.5	109.3	33.7
	D50	274.9	215.6	142.8	104.8	32.5
	D70	219.2	197.5	134.8	86.6	30.8
	D90	192.7	178.2	114.2	84.8	25.7
380×570×4	D0	283.8	220.8	171.0	101.1	32.5
	D20	282.5	221.2	169.9	100.4	32.2
	D50	253.7	197.0	150.7	85.3	27.0
	D70	230.8	184.1	141.3	79.7	24.7
	D90	209.8	164.4	125.2	68.9	21.4
380×570×2	D0	78.0	60.8	47.0	27.8	8.9
	D20	77.9	61.4	47.3	28.0	9.0
	D50	77.4	60.4	45.6	27.7	8.7
	D70	75.6	59.1	45.6	26.9	8.6
	D90	69.3	54.4	42.2	24.4	7.7

Failure Mode

The typical ultimate failure mode that occurs in the numerical specimen can be seen in Figure 7 and Figure 8. The title of the figures has specimen numbering, which involves the cross-section sizes (H×B×t) followed by the percentage of hole diameter and temperature simulation. The two figures show that the maximum yielding occurs in the upper flange of the sections due to local buckling generated from compression-flexure stresses experienced by the profile. No cross-sectional deformations occurred at the supports and the two loading points due to the coupling constraints activated in ABAQUS. Failure due to shear was not found in all numerical analysis results in ABAQUS.

Moment Versus Curvature Curve

Figure 9 and Figure 10 show the moment versus curvature curve of RHS 300×120×2 for different hole sizes and temperature variations for reference. As the temperature increases, the ultimate bending moment value decreases in both figures. Meanwhile, the corresponding curvature at the peak of the curves constantly decreases only in Figure 10 but not in Figure 9 as the temperature rises. The slope of the moment versus curvature ratio between sections without a hole and sections with a hole are quite different, where the latter is steeper than the former.
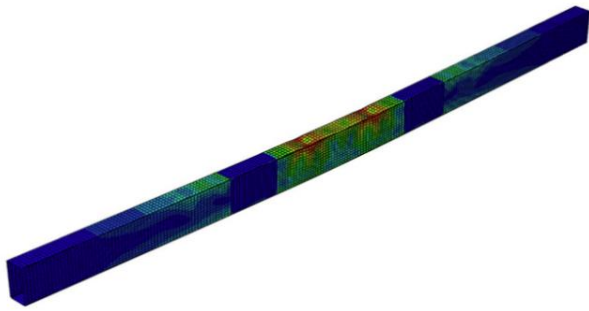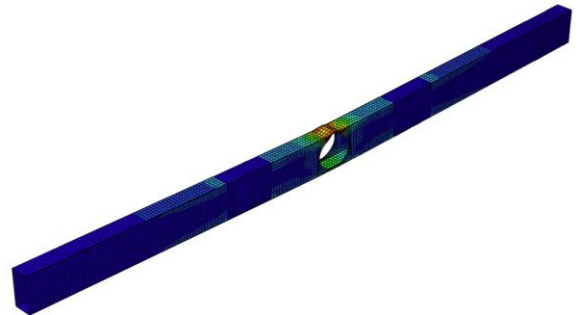
Figure 7. Failure Mode RHS 300×120×2D0T24
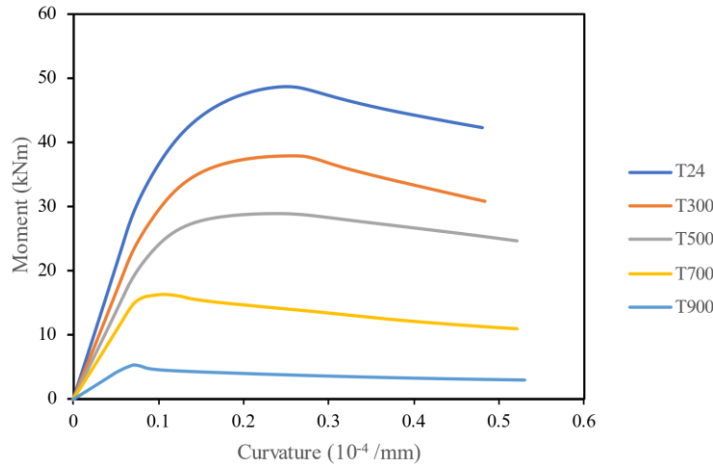

Figure 8. Failure Mode RHS 300×120×2D90T24

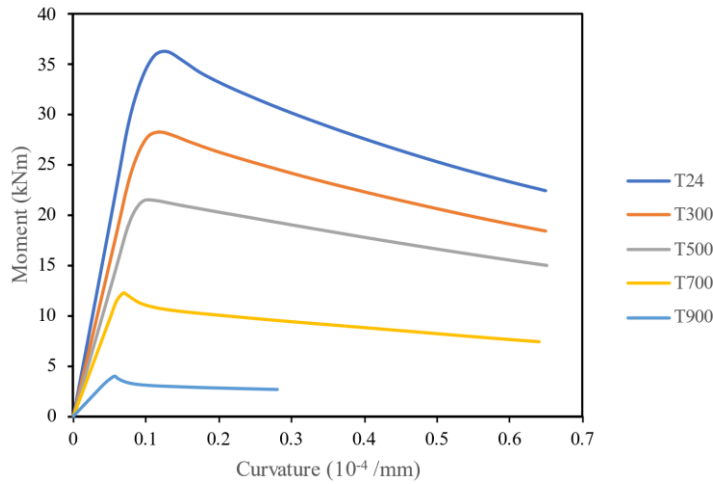**Figure 9.** Moment versus Curvature Curve of L300×120×2D0 at Elevated Temperatures

Figure 10. Moment versus Curvature Curve of L300×120×2D90 at Elevated Temperatures

Suitability of Bending Strength Equations

The M_{ult} values (in Table 5) are compared with the nominal bending strengths obtained from Equations (13) – (19) to evaluate the existing strength predictions. Additionally, further evaluation was carried out on the proposed strength equations as written in Equations (21) and (22). The proposed strength equations are formed based on the modification to the existing strength equations. The safety of the equations is evaluated and compared with the existing strength equations.

$$\lambda_l \leq 0.667, M_{nl} = (1.4 - 1\lambda_l)M_{ne} \qquad (21)$$

$$\lambda_l > 0.667, M_{nl} = \left[0.8 - 0.2\left(\frac{M_{crl}}{M_{ne}}\right)^{0.4}\right]\left(\frac{M_{crl}}{M_{ne}}\right)^{0.4} M_{ne} \qquad (22)$$

Table 6 presents a summary of the comparison results. Values obtained from a set of equations prescribed by ASCE [10] are denoted as M_{ASCE}, values from a set of equations from Chen et al. [5] are denoted as $M^{\#}_{DSM}$, and values from the proposed equations are denoted as M_{prop}. The average value (mean) and coefficient of variation (COV) between

M_{ult} and nominal capacity resulting from the M_{prop} equation produce the most conservative value because it has the largest mean value. It shall be noted that the ϕ value for M_{prop} is the highest, which means the equation is the least conservative one. Table 6 also shows the M_{prop} equation meets the minimum reliability index because the β_o is above 2.5 for RHS nonperforated and perforated sections. Even though the mean and COV values of $\frac{M_{ult}}{M^{\#}_{DSM}}$ are relatively small, $M^{\#}_{DSM}$ is not reliable because the β_o results on D20-D90 variation do not reach 2.5.

In addition to ASCE's reliability analysis, additional evaluation of safety criteria according to Kruppa [19] was carried out, as also conducted by Huang et al. [17]. This evaluation is applied to structures that are exposed to fire. The following evaluation criteria must be met to conclude the strength prediction is safely used:
1. The mean value of the ultimate to predicted bending strength ≥ 1.
2. The percentage for ultimate to predicted bending strength < 1 must be less than 20%.
3. The least value of the ultimate to predicted bending strength shall be > 0.85.

Table 6. Results from Reliability Analysis

	$\dfrac{M_{ult}}{M_{ASCE}}$			$\dfrac{M_{ult}}{M^{\#}_{DSM}}$			$\dfrac{M_{ult}}{M_{prop}}$		
	D0	D20-D90	D0-D90	D0	D20-D90	D0-D90	D0	D20-D90	D0-D90
Amount of data	40	160	200	40	160	200	40	160	200
Mean	1.23	1.13	1.15	1.14	1.03	1.05	1.48	1.34	1.37
COV	0.178	0.195	0.194	0.115	0.136	0.138	0.119	0.142	0.143
ϕ	0.9	0.9	0.9	0.9	0.9	0.9	0.95	0.95	0.95
β_o	2.87	2.50	2.57	2.97	2.48	2.56	3.78	3.26	3.33
% ratio <1	2.5%	31.25%	25.5%	17.5%	49.38%	43%	0%	1.25%	1%
Smallest ratio	0.98	0.76	0.76	0.95	0.74	0.74	1.2	0.98	0.98

Results from the evaluation using Kruppa's method show that the existing M_{ASCE} and $M^{\#}_{DSM}$ are not safely used since none of the requirements can be fulfilled for both perforated and non-perforated sections. Meanwhile, the proposed strength prediction fulfils the three requirements, and it is concluded that the proposed strength prediction is safely used to estimate the bending strength of RHS lean duplex beams at elevated temperatures.

In addition to the evaluation results presented in Table 6, Figure 11 presents the plot between M_{ult}/M_{ne} against the λ_l in comparison with three DSM curves (M_{ASCE}, $M^{\#}_{DSM}$, and M_{prop}). The figure also shows that the DSM curves plotted from M_{prop} design equations are located below the ratio of M_{ult}/M_{ne}. This confirms that the M_{prop} equations give the most conservative strength prediction.
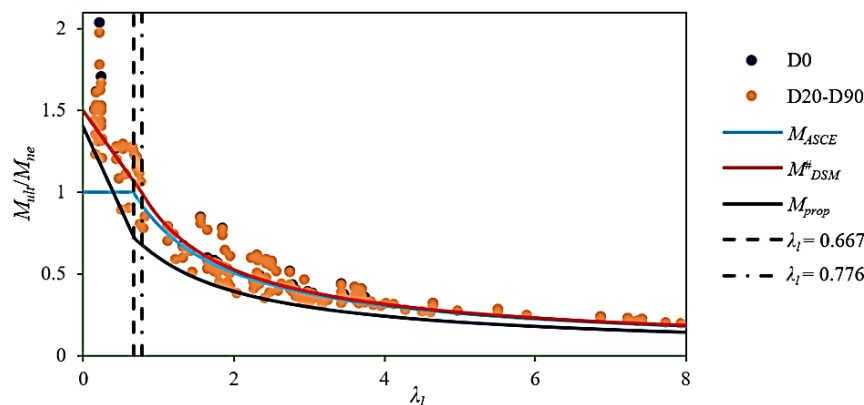
Figure 11. Three DSM Curves (M_{ASCE}, $M^{\#}_{DSM}$ dan M_{prop}) Plotted with M_{ult}/M_{ne}

Conclusions

A numerical investigation to evaluate the existing and proposed strength predictions is presented in this study. The evaluations were based on the comparison between ultimate strengths obtained from ABAQUS and the nominal strengths provided by the equations. Two hundred numerical specimens were built in ABAQUS to generate the parametric study, followed by the evaluation. The study included the flexural strength of the perforated beam at various hole sizes and temperature simulations. The existing strength predictions are not explicitly intended for the

perforated beam at elevated temperatures. However, results from the ASCE's reliability analysis shows that the three strength predictions are safely used for strength prediction of perforated beams at elevated temperatures, in general; it can be seen from the β_o values that are close to or above 2.50. Further evaluation shows only the proposed strength predictions from this study that satisfy the safety criteria for structures at elevated temperature as prescribed by Kruppa's method. Therefore, the application of the proposed strength prediction is recommended.

Acknowledgements

References

1. Yu, W.W., LaBoube, R.A., and Chen, H., *Cold-formed Steel Design*, Fifth edition, John Wiley & Sons, Hoboken, New Jersey, 2020.
2. Huang, Y. and Young, B., Stress-strain Relationship of Cold-formed Lean Duplex Stainless Steel at Elevated Temperatures, *Journal of Constructional Steel Research, 92*, 2014, pp. 103-113. https://doi.org/10.1016/j.jcsr.2013.09.007
3. Backhouse, A. and Baddoo, N., Recent Developments of Stainless Steels in Structural Applications, *Ce/papers, 4*(2-4), 2021, pp. 2349-2355. https://doi.org/10.1002/cepa.1560
4. Baddoo, N. R. and Francis, P., Development of Design Rules in the AISC Design Guide for Structural Stainless Steel, *Thin-Walled Structures, 84,* 2014, pp. 393-405. https://doi.org/10.1016/j.tws.2014.02.007
5. Chen, Z., Huang, Y., and Young, B., Design of Cold-formed Ferritic Stainless Steel RHS Perforated Beams, *Engineering Structures, 250*, 2022, 113372. https://doi.org/10.1016/j.engstruct.2021.113372
6. Chen, J. and Young, B. Stress-strain Curves for Stainless Steel at Elevated Temperatures, *Engineering Structures, 28*(2), 2006, pp. 229-239. https://doi.org/10.1016/j.engstruct.2005.07.005
7. Liu, Q., Sadowski, A. J., and Rotter, J. M., Ovalization Restraint in Four-Point Bending Tests of Tubes, *Journal of Engineering Mechanics, 145*(3), 2019, 04019009. https://doi.org/10.1061/(ASCE)EM.1943-7889.0001571
8. Robinson, P., A Concept for Experimentally Evaluating the Effect of Friction in the 4-ENF Interlaminar Toughness Test, *International Journal of Fracture, 110*, 2001, pp. 37-42. https://doi.org/10.1023/A:1012269526170
9. Chan, T. M. and Gardner, L., Bending Strength of Hot-rolled Elliptical Hollow Sections, *Journal of Construction Steel Research, 64*(9), 2008, pp. 971-986. https://doi.org/10.1016/j.jcsr.2007.11.001
10. SEI/ASCE 8, *Specification for the Design of Cold-formed Stainless Steel Structural Members*, American Society of Civil Engineers, 2022.
11. Prabowo, A., Introducing the Calculation Methods of Cold-formed Steel Member Strength, *Proceedings of KoNTekS 16*, Bali, Indonesia, October 27-28, 2022, ST-28.
12. Schafer, B.W., Review: The Direct Strength Method of Cold-formed Steel Member Design, *Journal of Constructional Steel Research*, *64*(7), 2008, pp. 766-778. https://doi.org/10.1016/j.jcsr.2008.01.022
13. Schafer, B. W. and Ádány, S., Buckling Analysis of Cold-formed Steel Member using CUFSM: Conventional and Constrained Finite Strip Methods, *Eighteenth International Specialty Conference on Cold-Formed Steel Structures*, Orlando, Florida, October 26-27, 2006.
14. Prabowo, A., Wijaya, H., Priestley, K.A., and Jonathan, *A Procedure to Compute the Nominal Strength of Cold-formed Perforated Stainless Steel Beams using Direct Strength Method*, Department of Civil Engineering, Universitas Tarumanagara, Jakarta, Report, 2023.
15. AISI S100-16, *North American Specification for the Design of Cold-formed Steel Structural Members*, American Iron Steel Intitute, 2016.
16. ABAQUS, *User's Manual and Theory Manual*, Dassault Systèmes Simulia Corp, 2023.
17. Huang, Y., Chen, J., He, Y., and Young, B., Design of Cold-formed Stainless Steel RHS and SHS Beam-columns at Elevated Temperatures, *Thin-Walled Structures, 165*, 2021, 107960. https://doi.org/10.1016/j.tws.2021.107960
18. Li, Q. Y. and Young, B., Structural Performance of Cold-formed Steel Built-up Section Beams under Non-uniform Bending, *Journal of Constructional Steel Research, 189*, 2022, 107050.
19. Kruppa, J., Eurocode Fire Parts: Proposal for a Methodology to Check the Accuracy of Assessment Methods, in *CEN TC 250*, Horizontal Group Fire, 1999, pp. 99-130.